NANO LETTERS

LETTER

pubs.acs.org/NanoLett

Built-in Electric Field Minimization in (In, Ga)N Nanoheterostructures

Zhiwen Liang,[†,‡] Isaac H. Wildeson,[§,‡] Robert Colby,[†,‡] David A. Ewoldt,[†,‡] Tong Zhang,[∥] Timothy D. Sands,[†,‡,§] Eric A. Stach,[†,‡] Bedrich Benes,[∥] and R. Edwin García*[,†,‡]

[†]School of Materials Engineering, [‡]Birck Nanotechnology Center, [§]School of Electrical and Computer Engineering, and [∥]College of Technology, Purdue University, West Lafayette, Indiana 47907, United States

Supporting Information

ABSTRACT: (In, Ga)N nanostructures show great promise as the basis for next generation LED lighting technology, for they offer the possibility of directly converting electrical energy into light of any visible wavelength without the use of down-converting phosphors. In this paper, three-dimensional computation of the spatial distribution of the mechanical and electrical equilibrium in nanoheterostructures of arbitrary topologies is used to elucidate the complex interactions between geometry, epitaxial strain, remnant polarization, and piezoelectric and dielectric contributions to the self-induced internal electric fields. For a specific geometry—nanorods with pyramidal caps—we demonstrate that by tuning the quantum well to cladding layer thickness ratio, h_w/h_c, a minimal built-in electric field can be experimentally realized and canceled, in the limit of $h_w/h_c = 1.28$, for large h_c values.

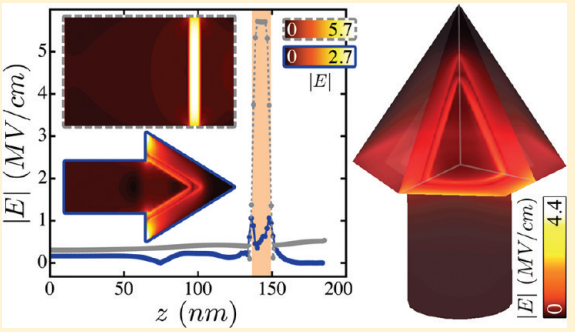

KEYWORDS: (In, Ga)N nanostructures, Stark effect, (In, Ga)N pyramids, strain-induced polarization

Light emitting diodes (LEDs) based on (In, Ga)N have recently received a great deal of attention due to their potential to deliver highly efficient light emission across the entire visible spectrum without the use of phosphors.[1−4] The realization of such a technology has been hampered by dislocations,[5−9] phase segregation,[10−12] and piezoelectric and spontaneous polarization fields.[13,14] In particular, the normal component of the polarization induces discontinuities across the interfaces of the quantum well heterostructures and gives rise to built-in electric fields that separate the injected electrons and holes and reduce the recombination probability. Such an effect is known as the quantum confined Stark effect (QCSE)[15−18] and is believed to be one of the main limitations hindering further efficiency improvement.[1−3] Conventional thin film heterostructures grown on polar (0001) planes possess electric fields in their quantum wells with magnitudes on the order of MV/cm, and this effect has driven research on nonpolar and semipolar heterostructures.[19−23] Recent investigations of nano- and microsized semipolar structures demonstrate the possibility of suppressing the built-in electric fields by engineering the quantum well geometry.[24−27] Among these novel designs, LED heterostructures grown on pyramidal nanorods with six semipolar $(1\bar{1}01)$-type facets show great promise with their low-cost fabrication based on template-assisted organometallic vapor phase epitaxy,[29,30] dislocation-free recombination regions,[6,7] and low elastic stresses allowing for a larger lattice mismatch before the incorporation of a misfit dislocation.[29] In this Letter, we demonstrate the possibility of dramatically reducing the QCSE within nanopyramid heterostructures. A window of realizable geometrical parameters that will lead to electric field-free (In, Ga)N active regions is quantified. Notably, this approach is generalizable and can be applied to other III−V nanostructured materials to more deeply understand the interplay between nanoscale geometry and relevant physical properties.

In order to address the coupled effects of polarization and stress, the mechanical and electrical equilibrium are simultaneously taken into account by solving the force balance equation and Coulomb's law in its differential form:

$$\nabla \cdot \vec{D} = \rho \tag{1}$$

$$\nabla \cdot \vec{\vec{\sigma}} = \vec{0} \tag{2}$$

in which $\vec{D}$ is the electric displacement vector and $\vec{\vec{\sigma}}$ is the stress tensor. $\vec{D}$ embodies contributions from dielectric polarization, $P_i^{Di} = \epsilon_{ij}E_j$, piezoelectric polarization, $P_i^{PZ} = d_{ijk}\sigma_{jk}$, and spontaneous polarization, P_i^{SP}, i.e.,

$$D_i = \epsilon_{ij}E_j + d_{ijk}\sigma_{jk} + P_i^{SP} \tag{3}$$

in which ϵ_{ij} is the dielectric permittivity, E_j is the electric field, and d_{ijk} is the piezoelectric tensor. σ_{ij} is a result of lattice mismatch from the heterostructure as well as the converse piezoelectric effect and described by

$$\sigma_{ij} = C_{ijkl}[\varepsilon_{kl}^{total} - \beta_{kl}(c - c_0) - d_{mkl}E_m] \tag{4}$$

Received: December 21, 2010
Revised: September 12, 2011
Published: September 26, 2011

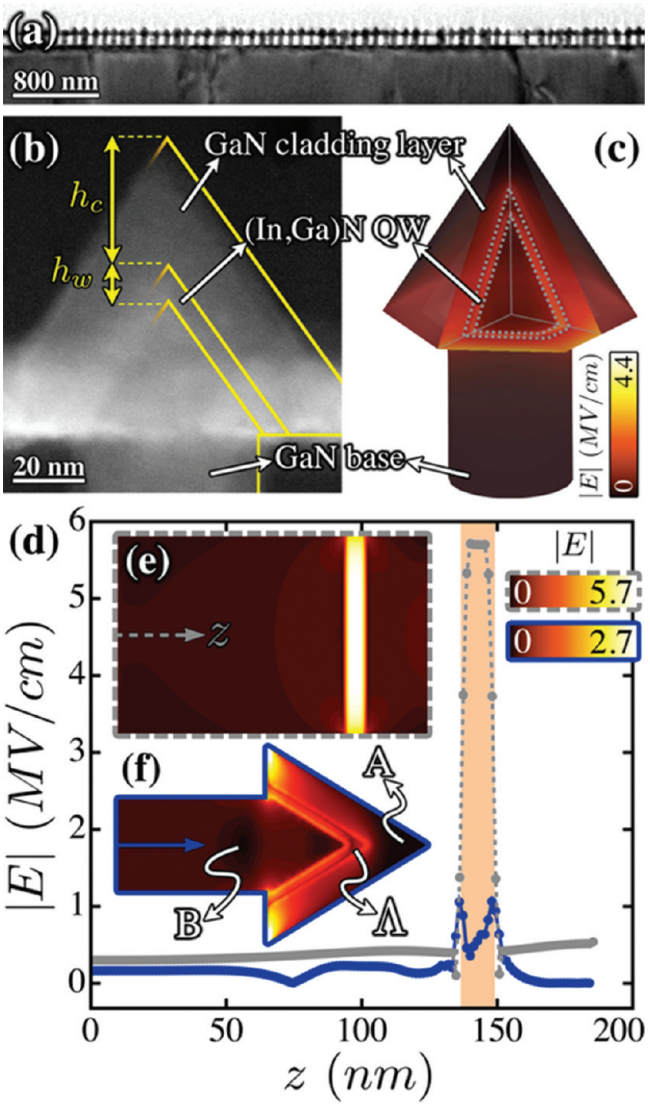

Figure 1. (a) A nanorod array as observed by transmission electron microscopy. (b) A single pyramidal nanorod imaged by annular dark field scanning transmission electron microscopy illustrating a GaN base, an (In, Ga)N quantum well, and a GaN cladding layer. The boundaries of each phase have been highlighted by yellow lines in half of the structure. (c) Three-dimensional electric field magnitude, $|E|$, distribution within a nanopyramid heterostructure containing an $In_{0.32}Ga_{0.68}N$ quantum well. (d) $|E|$ along the central z axis for both nanorod and thin film heterostructures. The shaded region of the plot corresponds to the $In_{0.32}Ga_{0.68}N$ quantum well. (e) Cross section of $|E|$ distribution for a corresponding thin film structure. (f) Cross section of $|E|$ distribution for the nanopyramid on a $(10\bar{1}0)$ plane. Region Λ highlights the low $|E|$ region within the quantum well, while regions A and B also show significant $|E|$ suppression.

C_{ijkl} is the stiffness tensor, $\varepsilon_{ij}^{\text{total}}$ is the total strain, β_{kl} is Vegard's tensor for the lattice misfit induced by the composition distribution in the heterostructure, and c_0 is the equilibrium stress-free composition.

The present framework includes the (solution to the homogeneous equation) remnant polarization, piezoelectric, and dielectric contributions to the electric fields and allows the effects of the depletion zone to be included, by explicitly introducing the position-dependent, electrostatic charge contributions

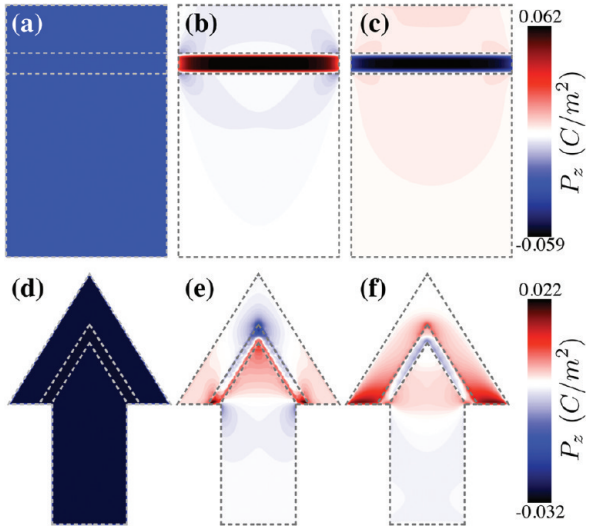

Figure 2. Individual polarization contributions (z component) for thin film (a−c) and pyramidal nanorod (d−f) heterostructures, each with an $In_{0.32}Ga_{0.68}N$ quantum well. Spontaneous polarization, P_z^{SP}, corresponds to insets (a) and (d), piezoelectric contributions, P_z^{PZ}, to insets (b) and (e), and dielectric contributions, P_z^{Di}, to insets (c) and (f).

(particular solution). Both contributions to the local electrostatic potential can be solved independently as readily described in standard textbooks.[28] In the present formulation, the focus is on describing the dipolar effects in the aforementioned pyramidal nanoheterostructures as a necessary step to suppress the QCSE.

Equations 1 through 4 were numerically solved by using the finite volume method. The simulated system was discretized into three-dimensional regular meshes. The largest simulated mesh had 3375000 elements, required 128 gigabytes of RAM, and 47 h of wall time on an Intel server with Red Hat Enterprise Linux 5 to converge. In the Supporting Information of this Letter, the developed model was validated by directly comparing the predicted built-in field against the analytical model as described by A. E. Romanov et al.[31]

In this Letter, the analyzed geometry is based on structures fabricated by Wildeson et al. using template-assisted organometallic vapor phase epitaxy.[29,30] A porous silica mask was used to grow arrays of pyramidal nanorods, each of which consists of a GaN base, an $In_{0.32}Ga_{0.68}N$ quantum well layer, and a GaN cladding layer (Figure 1a,b).

Panels c, d, and f of Figure 1 show a detailed view of the spatial distribution of the built-in electric field magnitude, $|E|$ within the pyramidal nanoheterostructure. While the thin film structure induces a high electric field of ∼5.7 MV/cm within the quantum well (Figure 1e), the nanopyramid design results in a reduced electric field within the recombination region (Figure 1f). Results show an extended area of low electric field magnitude, on the order of 0.5 MV/cm, in the vicinity of the apex of the pyramidal quantum well, labeled herein as region Λ. Moreover, the lowest value of $|E|$ = 0.34 MV/cm is found within the Λ region, which demonstrates more than an order of magnitude reduction compared to the thin film structure. Away from the tip, since only the components of the electric field that are normal to the heterointerface induce a spatial separation of the electrons and holes, the electric field magnitude serves as an upper bound

dx.doi.org/10.1021/nl1044605 |Nano Lett. 2011, 11, 4515–4519

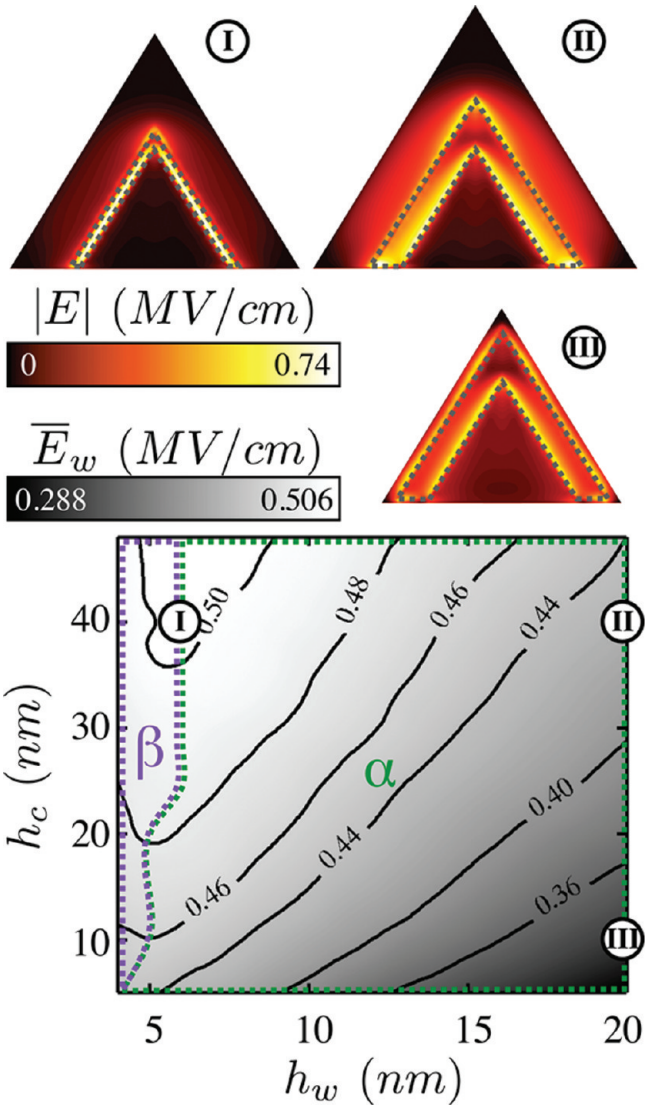

Figure 3. Isocontour map of the average electric field magnitude within an $In_{0.15}Ga_{0.85}N$ pyramidal quantum well, $\overline{E}_w$, as a function of the quantum well thickness, h_w, and the cladding layer thickness, h_c. $\overline{E}_w$ is a linear function of h_w/h_c within the regime outlined as α. Additional electric field reduction occurs in regime β because of the extremely thin quantum wells. Insets (I, II, and III) exemplify the electric field magnitude distributions for different h_w and h_c values.

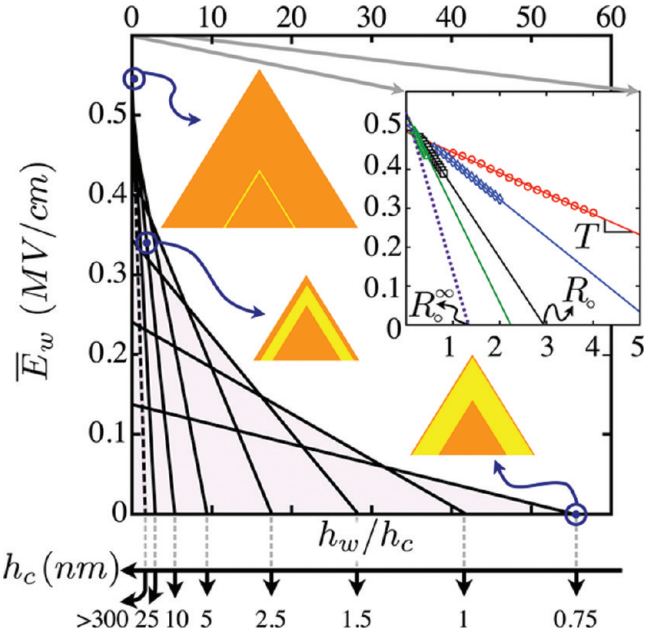

Figure 4. Average electric field magnitude within the $In_{0.15}Ga_{0.75}N$ pyramidal quantum well, $\overline{E}_w$, as a function of h_w/h_c for different h_c values. The enveloping curve of the lines in the plot shows that as the ratio of h_w/h_c increases, the maximum $\overline{E}_w$ decreases. Representative structures are shown. The dotted line corresponds to the thick cladding layer limit. In the inset, the red open circle corresponds to h_c = 5 nm, the blue open diamond corresponds to h_c = 10 nm, the black open square corresponds to h_c = 25 nm, while the green open triangle corresponds to h_c = 45 nm.

estimate on the QCSE. Thus, the electron and hole wave functions within a nanopyramid quantum well are expected to have an even greater overlap than what is predicted in this work. Other electric field suppressed regions include the apex of the GaN cladding layer, labeled as A in Figure 1f, and a volume along the nanorod axis a distance of 10 nm below the surface of the mask, labeled as B in Figure 1f. The highest electric field magnitude within the quantum well is found to be $|E|$ = 2.7 MV/cm, located near the bottom edge. However, the magnitude of the electric field in any of these locations is lower than its thin film counterpart due to the stress relaxation made possible by the larger surface to volume ratio of the pyramid geometry, which in turn greatly reduces the induced piezoelectric polarization.[29]

Figure 2 summarizes the individual contributions of polarization (z component) for both thin film and nanorod heterostructures. Results demonstrate that the piezoelectric contribution that results from the coherent lattice mismatch has the most control over the built-in electric field in the system. In comparison, the contributions from the spatial discontinuity of the spontaneous polarization are much smaller. Therefore, since the exterior surfaces of the nanopyramid relax the built-in stresses, the piezoelectric contribution is much lower than in a thin film, resulting in a nanopyramid LED with significantly suppressed electric field when engineered appropriately. From these results, we infer that it may be possible to significantly suppress electric fields in appropriately engineered LED structures.

Experimentally, the quantum well thickness, h_w, and the cladding layer thickness, h_c, within the nanopyramid heterostructures are two important parameters to be controlled during fabrication, and determine the average electric field magnitude within the quantum well, $\overline{E}_w$ (Figure 3). $\overline{E}_w$ is extracted within the upper 90% of the quantum well in order to avoid corner effects. Results show that thick cladding layers impose greater mechanical constraints on the quantum well and thus increase the piezoelectric polarization, which ultimately increases the electric field. Conversely, as the thickness of the cladding layer decreases, $\overline{E}_w$ is reduced. In the limit of thick quantum wells (the α regime), the larger (In, Ga)N volume allows further reduction in piezoelectric polarization, which in turn leads to $\overline{E}_w$ suppression. In the limit of thin quantum wells (the β regime), $\overline{E}_w$ is reduced because the stress state results in a favorable lowered level of piezoelectric polarization. Moreover, the electric field reduction is accompanied by an expansion of the Λ region from the apex down to the facets of the pyramidal quantum well (insets I, II, and III in Figure 3).

dx.doi.org/10.1021/nl1044605 |Nano Lett. 2011, 11, 4515–4519

In the α region, an empirical relationship between the built-in electric field and the nanopyramid geometry

$$\overline{E}_w = T\left(\frac{h_w}{h_c} - R_0\right) \text{ [MV/cm]}$$

is found, with an average deviation of 0.1% (Figure 4).

$$T = -\left(\frac{0.13}{h_c} + 0.55\right)/\left(\frac{40.54}{h_c} + 1.28\right) \text{ [MV/cm]}$$

represents the reduction rate of $\overline{E}_w$ with increasing h_w/h_c, and $R_0 = 40.54/h_c + 1.28$ corresponds to the ideal h_w/h_c ratio to specify an electric field-free structure. All possible geometries for $\overline{E}_w$ as a function of h_w/h_c are summarized in Figure 4. Each line corresponds to a fixed h_c and specifies an optimal ratio h_w/h_c, as denoted by R_0. As a result, the ensemble of the lines summarizes a series of optimal electric field-free geometries. The enveloping curve assembled by all of the lines (shaded area in Figure 4) embodies the range of built-in electric field values accessible by the pyramidal nanorod structures and suggests that as h_w/h_c increases, the highest possible built-in electric field is reduced. For $h_c \leq 1$ nm, $\overline{E}_w$ is suppressed to values under 0.25 MV/cm for all h_w/h_c. As h_c increases, a larger T suggests a more significant reduction rate of $\overline{E}_w$ as a function of h_w/h_c.

Current processing operations require thick cladding layers and thin quantum wells, which correspond to a maximum $\overline{E}_w$ = 0.55 MV/cm, a value much smaller than traditional thin film structures, which deliver $\overline{E}_w$ = 2.6MV/cm. As a result, even in the absence of any further topology engineering, (In, Ga)N pyramidal nanorods will suppress the QCSE by an order of magnitude. In the limit of thick cladding layers, $\overline{E}_w$ asymptotically approaches the expression (dotted line in Figure 4)

$$\overline{E}_w^{\infty} = -0.43\frac{h_w}{h_c} + 0.55 \text{ [MV/cm]} \quad (5)$$

For $h_c \geq 150$ nm, $\overline{E}_w$ and $\overline{E}_w^{\infty}$ differ from each other by less than 10%. Moreover, geometries displaying a zero built-in electric field are possible and correspond to quantum well and cladding layer thicknesses that satisfy the simple relation

$$R_0^{\infty} = \left.\frac{h_w}{h_c}\right|_{\text{optimal}} = 1.28 \quad (6)$$

Structures with such a thickness ratio may not be ideal from the perspective of a p−n junction device. Nevertheless, they provide insight that could be explored in other (In, Ga)N-based nanoheterostructures, potentially leading to geometries that completely eliminate polarization induced electric fields.

To summarize, we demonstrate that nanostructured (In, Ga)N-based pyramidal LEDs with semipolar facets reduce the built-in electric fields by 1 order of magnitude as compared to conventional thin film structures. Electric field magnitudes as low as 0.34 MV/cm are found within the apex of an $In_{0.32}Ga_{0.68}N$ nanopyramid quantum well, as compared to 5.7 MV/cm within a similar thin film heterostructure. Significantly reduced electric field magnitudes will alleviate the QCSE and result in more efficient LEDs. Moreover, it is demonstrated that the ratio of h_w/h_c controls the built-in polarization. In order to further suppress the built-in electric field, increasing the ratio of h_w/h_c is proposed. A set of optimal ratios are predicted to define electric field-free structures. In particular, in the limit of thick cladding layers, an optimal ratio of h_w/h_c = 1.28 will completely cancel the built-in electric field. Finally, while the predictions performed herein focus on a specific experimental geometry, they can be readily extended to describe other relevant three-dimensional nanoscale geometries in the III−V system,[32−34] micrometer-sized structures recently reported,[35] and even incorporate dislocation-free design ideas necessary in order to maximize the efficacy of the device.[7]

■ ASSOCIATED CONTENT

Supporting Information. Comparison of the predicted built-in field against the analytical model as described by Romanov et al. and a table of piezoelectric constants for GaN and InN. This material is available free of charge via the Internet at http://pubs.acs.org.

■ AUTHOR INFORMATION

Corresponding Author
*E-mail: redwing@purdue.edu.

■ ACKNOWLEDGMENT

Z.L. and R.E.G. acknowledge the support of the National Science Foundation, NSF DMR 0805022, and Advanced Materials. I.H.W. would like to acknowledge funding from the NDSEG research fellowship supported by the U.S. Department of Defense.

■ REFERENCES

(1) Nakamura, S. Current Status of GaN-Based Solid-State Lighting. *MRS Bull.* **2007**, *34*, 101107.
(2) Pimputkar, S.; Speck, J. S.; DenBaars, S. P.; Nakamura, S. Prospects for LED Lighting. *Nat. Photonics* **2009**, *3*, 180182.
(3) Nakamura, S.; Senoh, M.; Nagahama, S.; Iwasa, N.; Yamada, T.; Matsushita, T.; Kiyoku, H.; Sugimoto, Y.; Kozaki, T.; Umemoto, H.; Sano, M.; Chocho, K. Present Status of InGaN/GaN/AlGaN-Based Laser Diodes. *J. Cryst. Growth* **1998**, *189/190*, 820–825.
(4) Shchekin, O. B.; Krames, M. R.; Mueller-Mach, R.; Mueller, G. O.; Zhou, L.; Harbers, G.; Craford, M. G. Status and Future of High-Power Light-Emitting Diodes for Solid- State Lighting. *J. Disp. Technol.* **2007**, *3* (2), 160–175.
(5) Nakamura, S. The Roles of Structural Imperfections in InGaN-Based Blue Light- Emitting Diodes and Laser Diodes. *Science* **1998**, *281*, 956–961.
(6) Colby, R.; Liang, Z.; Wildeson, I. H.; Ewoldt, D. A.; Sands, T. D.; Stach, E. A.; García, R. E. Dislocation Filtering in GaN Nanostructures. *Nano Lett.* **2010**, *10*, 1568–1573.
(7) Liang, Z.; Colby, R.; Wildeson, I. H.; Ewoldt, D. A.; Sands, T. D.; Stach, E. A.; García, R. E. GaN Nanostructure Design for Optimal Dislocation Filtering. *J. Appl. Phys.* **2010**, *108*, 074313.
(8) Chichibu, S.; Azuhata, T.; Sota, T.; Nakamura, S. Spontaneous Emission of Localized Excitons in InGaN Single and Multiquantum Well Structures. *Appl. Phys. Lett.* **1996**, *69*, 4188–4190.
(9) Lester, S. D.; Ponce, F. A.; Craford, M. G.; Steigerwald, D. A. High Dislocation Densities in High Efficiency GaN-Based Light-Emitting Diodes. *Appl. Phys. Lett.* **1995**, *66*, 1249–1251.
(10) Han, B.; Wessels, B. W.; Ulmer, M. P. Investigation of Nanoscale Composition Fluctuations in InGaN Using Optical Transmission Spectroscopy and Near-Field Scanning Optical Microscopy. *J. Appl. Phys.* **2006**, *99*, 084312.
(11) Lin, Y. S.; Ma, K. J.; Hsu, C.; Feng, S. W.; Cheng, Y. C.; Liao, C. C.; Yang, C. C.; Chou, C. C.; Lee, C. M.; Chyi, J. I. Dependence of Composition Fluctuation on Indium Content in InGaN/GaN Multiple Quantum Wells. *Appl. Phys. Lett.* **2000**, *77*, 2988–2990.

(12) Liu, J. Z.; Zunger, A. Thermodynamic States and Phase Diagrams for Bulk-Incoherent, Bulk-Coherent, and Epitaxially-Coherent Semiconductor Alloys: Application to Cubic (Ga,In)N. *Phys. Rev. B* **2008**, *77*, 205201.

(13) Bernardini, F.; Fiorentini, V. Polarization Fields in Nitride Nanostructures: 10 Points to Think About. *Appl. Surf. Sci.* **2000**, *166*, 23–29.

(14) Chichibu, S. F.; Abare, A. C.; Minsky, M. S.; Keller, S.; Fleischer, S. B.; Bowers, J. E.; Hu, E.; Mishra, U. K.; Coldren, L. A.; Denbaars, S. P.; Sota, T. Effective Band Gap In Homogeneity and Piezoelectric Field in InGaN/GaN Multiquantum Well Structures. *Appl. Phys. Lett.* **1998**, *73*, 2006–2008.

(15) Miller, D. A. B.; Chemla, D. S.; Damen, T. C. Band-Edge Electroabsorption in Quantum Well Structures: The Quantum-Confined Stark Effect. *Phys. Rev. Lett.* **1984**, *53*, 2173–2176.

(16) Masui, H.; Sonoda, J.; Pfaff, N.; Koslow, I.; Nakamura, S.; DenBaars, S. P. Quantum- Confined Stark Effect on Photoluminescence and Electroluminescence Characteristics of InGaN-Based Light-Emitting Diodes. *J. Phys. D: Appl. Phys.* **2008**, *41*, 165105.

(17) Takeuchi, T.; Sota, S.; Katsuragawa, M.; Komori, M.; Takeuchi, H.; Amano, H.; Akasaki, I. Quantum-Confined Stark Effect due to Piezoelectric Fields in GaInN Strained Quantum Wells. *Jpn. J. Appl. Phys.* **1997**, *36*, L382–L385.

(18) Chichibu, S. F.; Abare, A. C.; Minsky, M. S.; Keller, S.; Fleischer, S. B.; Bowers, J. E.; Hu, E.; Mishra, U. K.; Coldren, L. A.; Denbaars, S. P. Effective Band Gap Inhomogeneity and Piezoelectric Field in InGaN/GaN Multiquantum Well Structures. *Appl. Phys. Lett.* **1998**, *73*, 2006.

(19) Chakraborty, A.; Haskell, B. A.; Keller, S.; Speck, J. S.; DenBaars, S. P.; Nakamura, S.; Mishra, U. K. Nonpolar InGaN/GaN Emitters on Reduced-Defect Lateral Epitaxially Overgrown a-Plane GaN with Drive-Current-Independent Electroluminescence Emission Peak. *Appl. Phys. Lett.* **2004**, *85*, 5143–5145.

(20) Chitnis, A.; Chen, C.; Adivarahan, V.; Shatalov, M.; Kuokstis, E.; Mandavilli, V.; Yang, J.; Khan, M. A. Visible Light-Emitting Diodes Using a-Plane GaN-InGaN Multiple Quantum Wells Over r-Plane Sapphire. *Appl. Phys. Lett.* **2004**, *84*, 3663–3665.

(21) Yamada, H.; Iso, K.; Saito, M.; Hirasawa, H.; Fellows, N.; Masui, H.; Fujito, K.; Speck, J. S.; DenBaars, S. P.; Nakamura, S. Comparison of InGaN/GaN Light Emitting Diodes Grown on m-Plane and a-Plane Bulk GaN Substrates. *Phys. Status Solidi RRL* **2008**, *2*, 89–91.

(22) Iso, K.; Yamada, H.; Hirasawa, H.; Fellows, H.; Saito, M.; Fujito, K.; DenBaars, S. P.; Speck, J. S.; Nakamura, S. High Brightness Blue InGaN/GaN Light Emitting Diode on Nonpolar m-Plane Bulk GaN Substrate. *Jpn. J. Appl. Phys.* **2007**, *46*, L960–L962.

(23) Zhong, H.; Tyagi, A.; Fellows, N. N.; Wu, F.; Chung, R. B.; Saito, M.; Fujito, K.; Speck, J. S.; DenBaars, S. P.; Nakamura, S. High Power and High Efficiency Blue Light Emitting Diodes on Free-Standing Semipolar $(10\bar{1}\bar{1})$ Bulk GaN Substrate. *Appl. Phys. Lett.* **2005**, *86*, 111101.

(24) Yu, H.; Lee, L. K.; Jung, T.; Ku, P. C. Photoluminescence Study of Semipolar $\{10\bar{1}1\}$ InGaN/GaN Multiple Quantum Wells Grown by Selective Area Epitaxy. *Appl. Phys. Lett.* **2007**, *90*, 141906.

(25) Nishizuka, K.; Funato, M.; Kawakami, Y.; Narukawa, Y.; Mukai, T. Efficient Rainbow Color Luminescence from $In_xGa_{1-x}N$ Single Quantum Wells Fabricated on $\{11\bar{2}2\}$ Microfacets. *Appl. Phys. Lett.* **2005**, *87*, 231901.

(26) Wunderer, T.; Lipski, F.; Schwaiger, S.; Hertkorn, J.; Wiedenmann, M.; Feneberg, M.; Thonke, K.; Scholz, F. Properties of Blue Green InGaN/GaN Quantum Well Emission on Structured Semipolar Surfaces. *Jpn. J. Appl. Phys.* **2009**, *48*, 060201.

(27) Pérez-Solórzano, V.; Gröning, A.; Jetter, M. Near-Red Emission from Site-Controlled Pyramidal InGaN Quantum Dots. *Appl. Phys. Lett.* **2005**, *87*, 163121.

(28) Strang, G. *Introduction to Applied Mathematics*; Wellesley-Cambridge Press: Wellesley, MA, 1986.

(29) Wildeson, I.; Colby, R.; Ewoldt, D.; Liang, Z.; Zakharov, D. N.; Zaluzec, N. J.; García, R. E.; Stach, E. A.; Sands, T. D. III-Nitride Nanopyramid LEDs Grown by Organometallic Vapor Phase Epitaxy. *J. Appl. Phys.* **2010**, *108*, 044303.

(30) Deb, P.; Kim, H.; Rawat, V.; Oliver, M.; Kim, S.; Marshall, M.; Stach, E. A.; Sands, T. D. Faceted and Vertically Aligned GaN Nanorod Arrays Fabricated without Catalysts or Lithography. *Nano Lett.* **2005**, *5*, 1847–1851.

(31) Romanov, A. E.; Baker, T. J.; Nakamura, S.; Speck, J. S. Strain-Induced Polarization in Wurtzite III-Nitride Semipolar Layers. *J. Appl. Phys.* **2006**, *100*, 023522.

(32) Su, J.; Cui, G.; Gherasimova, M.; Tsukamoto, H.; Han, J.; Ciuparu, D.; He, Y.; Nurmikko, A. V.; Broadbridge, C.; Lehman, A. Catalytic Growth of Group III-Nitride Nanowires and Nanostructures by Metalorganic Chemical Vapor Deposition. *Appl. Phys. Lett.* **2005**, *86*, 013105.

(33) Lim, S. K.; Brewster, M.; Qian, F.; Li, Y.; Lieber, C. M.; Gradecak, S. Direct Correlation Between Structural and Optical Properties of III-V Nitride Nanowire Heterostructures with Nanoscale Resolution. *Nano Lett.* **2009**, *9*, 3940–3944.

(34) Dong, Y.; Tian, B.; Kempa, T. J.; Lieber, C. Coaxial Group III-Nitride Nanowire Photovoltaics. *Nano Lett.* **2009**, *9*, 2183–2187.

(35) Hsu, C.-W.; Lundskog, A.; Karlsson, K. F.; Forsberg, U.; Jansén, E.; Holtz, P. O. Single Excitons in InGaN Quantum Dots on GaN Pyramid Arrays. *Nano Lett.* **2011**, *11*, 2415–2418.